The Iraqi Journal for Mechanical and Material Engineering, Vol.25, No 2, June 2026

ISSN: 1819-2076; eISSN: 2313-3783

BENCHMARKING PERVAPORATION MEMBRANES FOR FUEL DESULFURIZATION: A FLUX–ENRICHMENT FACTOR TRADE-OFF ANALYSIS

Yasir A. Al-kawaz[1*], Auda J. Braihi[2], Ali S. Hasan[3]

[1,2,3] Department of Polymer and Petrochemical Industries, University of Babylon, Babylon, Iraq
***Corresponding author: eng.yasir.alkawaz@gmail.com**

ABSTRACT

Due to increased stringent emission regulations and the declining availability of low-sulfur crude oil have created an urgent need for advanced fuel desulfurization technologies. Among emerging approaches, pervaporation (PV) using membrane separation at mild operating conditions has gained recognition as a promising alternative to conventional methods. However, wide variations in reported operating parameters and testing conditions make direct comparison of membrane performance challenging. In this study, pervaporative desulfurization data from four published works (covering 10 membrane configurations) were systematically normalized and evaluated using design maps and Pareto-front analysis. To ensure fair comparison, two standardized operating windows were defined: (A) thiophene/n-octane at 30 ± 5 °C and (B) thiophene/n-heptane at 60 ± 5 °C, both at sulfur concentrations of 400–600 ppm. Membrane performance was assessed by jointly considering total flux and enrichment factor (EF), enabling identification of non-dominated configurations. In Window A, PDMS/MIL-101(Cr) (6 wt%) exhibited the most favorable flux–selectivity balance, achieving approximately 5.2 kg $m^{-2} h^{-1}$ flux and an EF of ~5.6. A simplified stage-cut mass balance further linked EF to practical sulfur reduction in the retentate. Despite the limited dataset, the proposed framework provides a transparent, reproducible benchmarking methodology to support rational membrane selection and design for fuel desulfurization.

Keywords: Pervaporation, Desulfurization, Design maps, Pareto frontier, Zeolite.

NOMENCLATURE

J	Total flux
J_i	Flux of component *i*
m_i	Collected permeate mass of component *i*
A	Membrane area
t	Time

Received: November 30, 2025.
Accepted: April 9, 2026.

Publisher: University of Babylon / Faculty of Engineering
Journal homepage: https://www.iqjfmme.com

y_i	Mass (or mole) fraction of component *i* in permeate
θ	Stage-cut (permeate/feed mass ratio)
C_f	Feed sulfur concentration
C_p	Permeate sulfur concentration
C_r	Retentate sulfur concentration
P_i	Permeability
L_i	Permeance
l	Selective-layer thickness
Δp_i	Partial-pressure driving force
x_i	Liquid mole fraction in feed
a_i	Activity
γ_i	Activity coefficient
P_i^0	Saturated vapor pressure
P_p	Permeate-side pressure
EF	Enrichment factor

1. INTRODUCTION

Desulfurizing of gasoline and diesel fuels is a major global environmental issue as well as an industrial requirement. These chemicals are responsible for significant environmental pollution and the corrosion of automobile engines. On the other side, emitted sulfur oxide (SOx) is produced by burning fuels that contain sulfur and it leads acid rain and damages of life phenomena on both living beings and human health Mamuad and Choi [1] . Furthermore, sulfur deactivates catalysts in vehicle exhaust which may make the reduction of other pollutants less efficient Esmaeili-Faraj *et al.*, [2]. This issue has been further intensified due to imposition of stringent environmental legislation such as sulfur content in gasoline less than 10 ppm which made the problem more difficult Mortaheb *et al.*,[3,4] . In such a situation, pervaporation (PV), namely a thin film membrane separation process for differential transport through a dense membrane with subsequent phase change on the permeate side under vacuum condition. The pervaporation (PV) is based on the different adsorbability and diffusivity of the components through a non-porous selective membrane Salman *et al.*, [5]. The process is conducted under the influence of a chemical potential difference which is typically effected by continuously withdrawing the permeate compounds from the permeate side with vacuum or evacuation in combination with a sweeping gas. PV emerged be a candidate technology for removing for removing sulfur compounds from fuels. This membrane-based process provides an effective and sustainable solution for removing sulfur compounds in the petrochemical industry Hong *et al.*,[6] . In contrast to the classical separation techniques such as hydrodesulfurization, liquid–liquid extraction, and adsorption in terms of selectivity, separation efficiency and energy consumption, Pervaporation (PV) exhibit lower energy requirements that has more merits

compared with the other conventional desulfurization process though it occurs at relatively mild conditions pervaporation is favored over aromatic sulfur compounds. These properties make pervaporation particularly good choice for the deep desulfurization of transportation fuels which becomes more important when ultra-low sulfur is required. Han *et al.*,[7].

Several researchers worked on the creation of desulfurization membranes. Polymers are being studied for application of the membranes in separation. These are with polydimethylsiloxane (PDMS), polyethylene glycol (PEG) and polyimide (PI), which have been reported to have higher permeability and processability Cai *et al.*,[8-10] . The mixed matrix membranes (MMMs) can be prepared by addition of inorganic fillers, containing metal-organic frameworks (MOFs), zeolites, and silver-based additives into polymer matrixes with better performance for the anti-biofouling properties membrane including these materials Cai *et al.*[8,11,12,13,14]. Nevertheless, due to the wide variety of different materials and fabrication techniques available, it is hard to evaluate which type has more efficiency based on some comparative standard. Literature data on the pervaporation desulfurization have been reported under a wide range of operating conditions such as various kinds and concentrations of sulfur compounds, hydrocarbons, temperatures, pressures, membrane thicknesses. According to Kadhum *et al.* [15] the difference in so many parameters makes that to compare obtained results for a specific membrane with the others which developed in completely other conditions not reasonable. Therefore, it is difficult to directly compare distinct membranes. Furthermore, the performance of membranes is influenced by the balance between rate of flow (flux) and component separation ability (selectivity); thus an improvement in one will result in a decrease in another Park *et al.*,[16,17] . Therefore, using only one parameter to assess membrane performance may lead to an inaccurate interpretation of the data. To tackle these issues, it is essential to develop an integral and impartial approach, allowing a fair comparison of membrane performance between heterogeneous datasets. In this respect, design space maps and Pareto front analysis are useful tools for visually representing performance trade-offs and discovering non-dominated membrane configurations that offer optimized compromises between productivity and separation efficiency Hara *et al.*,[18] .

The originality of this work is to develop a unified model based on a statistical analysis of available data published on pervaporation desulfurization process. The goal of this approach is to uniformly correlate the properties of membranes with their separation performance and uncover relevant structure-activity relationships. The highly correlated relationships of membrane properties (e.g., composition, surface functionalization, etc.) and the operating conditions (like temperature, sulfur feed concentration, pressure) to the key performance metrics (flux and enrichment gap) are abstracted into pairwise distributions for design map generation. These maps are excellent, mnemonic, conflict-free guides to trouble-shooting and optimizing your membrane. The use of the Pareto front approach is extended as a tool to investigate efficient, non-dominated membrane structures displaying an optimal balance between flux and selectivity. Taken together, this study presents a general benchmarking protocol for the pervaporation-based fuel desulfurization membranes by comparatively collecting performance data reported in literature under fixed relative operation windows towards fair and reliable comparisons among different membrane materials and system designs.

2. THEORITICAL PART

2.1. Data collection criteria

The database utilized in this research work was constructed based on the detailed evaluation of peer-reviewed journal articles containing investigations into pervaporation process for membrane-based fuel desulfurization and systematically structured. Only those studies that included full and eligible quantitative measure of performance were considered. These input variables include feed sulfur concentration (C_{feed}), either permeate sulfur concentration (C_{perm}) or enrichment factor (EF), total permeate flux and operating temperature with n-alkane media. Articles with non-pervaporation research or insufficient data (with an emphasis on EF and flux values) were excluded for the sake of consistency and reliability of comparative analysis. Borderline entries (e.g., thickness "~14 μm", vacuum "<3 mbar") were retained with the qualifier recorded Wang *et al.*,[10,19,20] . Screening flow and counts are presented in PRISMA‑ style selection diagram as in fig.1. Studies on other desulfurization techniques (adsorption, liquid–liquid extraction, or hydrodesulfurization) were not considered. Experiments lacking a necessary performance criteria, without full descriptions of the operating conditions or with data points not within given, experimentally determined assessing windows were excluded. This eligibility criterion was applied in order to maintain uniformity and reduce bias, thus allowing a fair comparison between membrane materials and experimental conditions across the different studies.

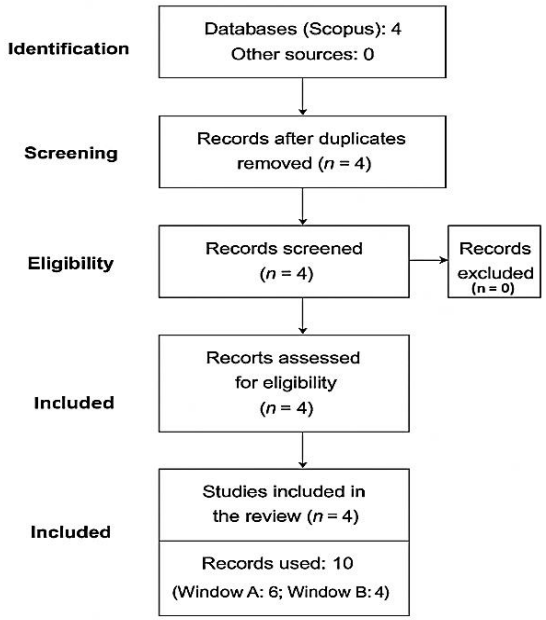

Fig.1. PRISMA‑ style selection diagram.

Sulfur concentrations were converted to ppm (mass basis; 1 weight percent = 10,000 ppm), and the total mass of the polymers, fillers, support structure, etc. was recorded in $kg \cdot m^{-2} \cdot h^{-1}$. All the original data from this paper was transformed into a standard format. The following metadata normalized to the schema: {Ref., polymer, support, filler, filler_wt_pct, sulfur_compound, model_fuel, feed_conc_ppm, permeate_conc_ppm,

temperature_c, permeate_pressure_mbar, thickness_um, and total_permeate_flux_kg_m2_h}.

2.2. Limitations related to data availability

The amount of data per window is inherently small and not uniform, but this simply represents the limited availability of some types of data in the literature rather than some form of selective sampling. Thus, the findings of this study do not attempt to generalize statistically inferential results but only relative and trend ratios from normalized and standardized data. The applied design map and Pareto front analyses are well suited to such datasets, allowing non-dominated performance trends to be identified without recourse to large numbers of evenly spaced samples.

2.3. Metrics and operating windows

Selectivity quantified as the enrichment factor (EF), defined on a mass-concentration basis as $EF = \frac{C_{perm}}{C_{feed}}$ (dimensionless). Flux was used as reported or converted to kg·m^{-2}·h^{-1}. To ensure comparability, all analyses confined to two fixed operating windows:

Window A: Thiophene / *n*-octane / 30 ± 5 °C / 400–600 ppm

Window B: Thiophene / *n*-heptane / 60 ± 5 °C / 400–600 ppm

The predefined operating windows were not designed to cover the entire range of fuel compositions, nor the range of pervaporation operating conditions found in an industrial setting. Instead, they were derived from the most common fuel system and operating conditions reported in pervaporation desulfurization literature where adequate and comparable datasets were available for comparison. The selected feed and permeate fuel systems and corresponding operating conditions cover the dominantly pervaporation mechanisms determining performance (adsorptive selectivity, diffusion-controlled permeation), which are mainly affected by temperature, sulfur compound type and membrane material. Therefore, the selected operating windows are sufficient to assess the relative effectiveness and comparative performance of various membranes in the framework of a benchmark study as opposed to an exhaustive comparison across all industrial operating scenarios.

Per-window subsets and sources appear in the Results (Table 1 for A; Table 4 for B).

Linking EF to fuel quality. We relate EF to the retentive sulfur level using a single-stage mass balance with stage-cut θ (permeate/feed mass). Let $\theta = \frac{J_{total} \cdot A}{F_{feed}}$. Then the retentate concentration and the percent reduction in the retentate are:

$$EF = \frac{C_{perm}}{C_{feed}} \quad (1)$$

$$J_T = \frac{m_p}{(A * t)} \quad (2)$$

$$J_i = \frac{m_I}{(A * t)} = J_T * w_i^p \quad (3)$$

$$\theta = \frac{(J_T * A)}{F_{feed}} \quad (4)$$

$$C_{ret} = \frac{(C_{feed} - theta * C_{perm})}{(1-\theta)} \quad (5)$$

$$Retentate\ removal\ (\%) = \left[theta * \frac{(EF-1)}{(1-\theta)} \right] * 100 \quad (6)$$

$$Permeance_i(\Pi_i) = \frac{J_i}{Delta_{p_i}} \quad (7)$$

$$Permeability_i(P_i) = \frac{(J_i * l)}{Delta_{p_i}} = D_i * S_i \quad (8)$$

$$Delta_{p_i} = a_i^f * p_i^{sat(T)} - y_i^p * P_{perm} \quad (9)$$

$$With\ a_i^f = \gamma_i * x_i^f\ and, under\ deep\ vacuum, Delta_{p_i} \approx a_i^f * p_i^{sat(T)}$$

J_T total flux; J_i flux of component *i*; m_p (m_i) collected permeate (component) mass; A membrane area; *t* time; $\frac{w_i^p}{y_i^p}$ mass/mole fraction of *i* in the permeate; θ stage-cut; C_{feed}, C_{perm}, $C_{ret}feed$/permeate/retentate concentrations; Π_i permeance; P_i permeability; l selective-layer thickness; $Delta_{p_i}$ partial-pressure driving force; x_i^f liquid mole fraction in feed; a_{if} activity; $\gamma_i a_i$ activity coefficient; p_i^{sat} saturated vapor pressure; P_{perm} permeate-side pressure.

2.4. Analysis workflow (uncertainty, trade‑offs, ranking, statistics)

Within each window, rows sharing the same configuration (polymer, filler, wt. %) were grouped; we report mean ± SD for Flux and EF. Error‑bar summaries appear below, and the corresponding table (uncertainty_by_configuration.csv) is provided as a machine‑readable file.

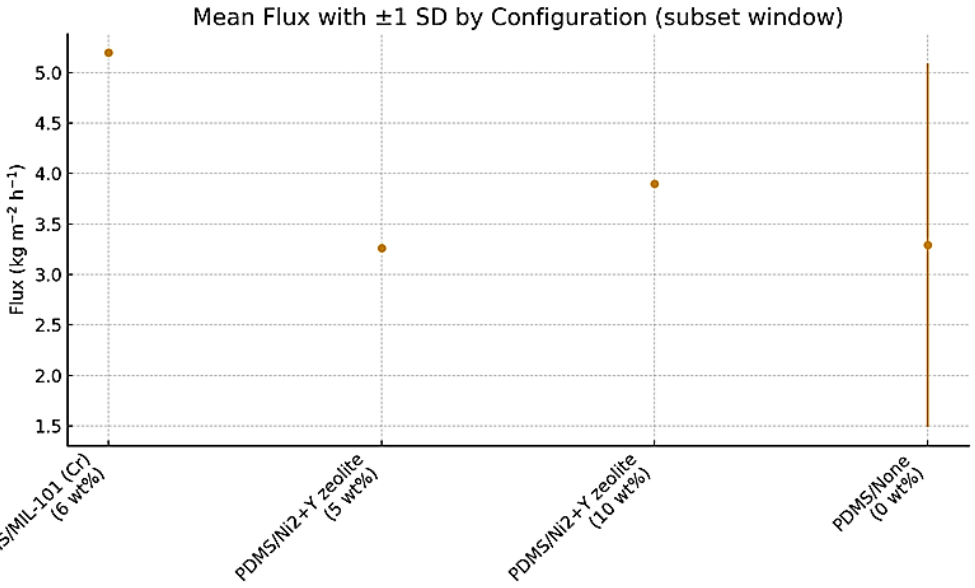

Fig.2. Mean Flux ± SD by configuration
Drop unc_Flux_error bars.

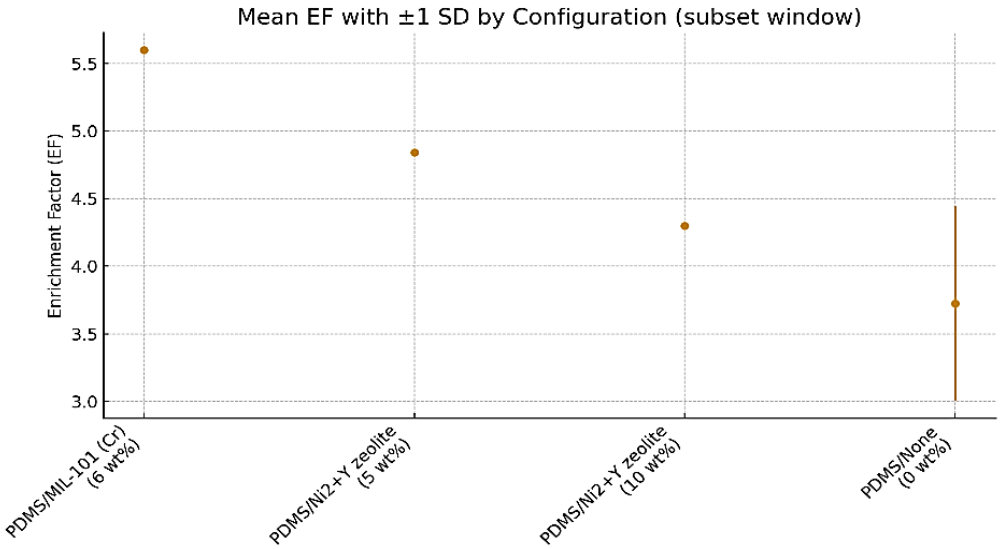

Fig.3. Mean EF ± SD by configuration
Drop unc_EF_error bars.

To visualize trade-offs, we plot Flux vs EF (design maps) and mark non-dominated (Pareto) points, where no other point improves both metrics simultaneously. For fast screening, the leader board score orders configurations by min–max-normalized mean product. Exploratory ordinary least squares (OLS) connects Flux or EF to filler loading (wt%), filler family (MOF; Zeolite/Ag; baseline = None), and a ceramic-support indicator, with 2,000 bootstrap resamples producing 95% CIs. In consideration of small sample sizes, coefficients have been interpreted as effect size estimates in the direction.

$$\text{mean}(X) = \left(\frac{1}{n}\right) * \Sigma_k X_k \tag{10}$$

$$\text{SD}(X) = \text{sqrt}\left[\left(\frac{1}{n-1}\right) * \Sigma_k \left(X_k - \text{mean}(X)\right)^2\right] \tag{11}$$

$$95\%\ \text{CI (normal approx)} = \text{mean}(X) \pm t_{0.975,n-1} * \frac{(\text{SD}(X))}{\text{sqrt}(n)} \tag{12}$$

$$X_{\text{tilde}} = \frac{(X - X_{\min})}{(X_{\max} - X_{\min})} \tag{13}$$

$$\text{Leaderboard score: } S = J_{\text{tilde}} * EF_{\text{tilde}} \tag{14}$$

(Computed on configuration-level means within each window)

Pareto dominance: at point a dominates b if [$J_a \geq J_b$ and $EF_a \geq EF_b$]and at least one strict (>)

$$Y \in \{\text{mean}(\text{Flux}), \text{mean}(EF)\} = \beta_0 + \beta_1 * \text{wt\%} + \beta_2 * I_{(\text{MOF})} + \beta_3 * I_{\left(\frac{\text{Zeolite}}{\text{Ag}}\right)} + \beta_4 * I_{(\text{Ceramic support})} + \varepsilon \tag{15}$$

wt.% is the additive mass fraction (continuous); I are binary indicators equal to 1 when the attribute is present and 0 otherwise. The intercept β0 corresponds to the expected value of mean (Flux) and mean (EF) for the baseline configuration (no MOF, no Zeolite/Ag, non-ceramic support) at wt.%=0. Therefore, β1 is the amount that we predict Y would increase by one wt.% increase of additive (while the other factors remain unchanged), where β1, β2, β3 and β4 are systematic shifts of capture related to MOF fillers, zeolites/silver additives and ceramic supports. Here ε is a random error. With this specification, we can estimate how average performance depends on the composition and support types when the tolerance to load is additive.

3. VISUALIZATION, TRANSPARENCY, AND CITATION

Matplotlib (version 3.0) used for generating results. We used embedded fonts and colorblind-friendly palettes to balance accessibility with publication quality. High-quality raster images were saved as PNG format (≥ 300 dpi). Where appropriate, bubble areas were normalized to the additive content (wt%) by a surface-area scaling and corresponding reference-values are indicated as legends (e.g., 0, 5, 10, 15 wt%). Axes are scaled in ons and citations to the original data sources are given below each volume bar. All data are accompanied by provenance metadata (Study_ID, PMID, Page_Figure) so that they can be traced back. Machine-readable outputs, including subset-specific CSV files, Pareto-front datasets, cross-validation leaderboards, uncertainty tables, and the full analytical workbook are stored using a standardized nomenclature and available with this publication. A README file, and a detailed instructions on computational environment (requirements.txt or environment.yml) are included to facilitate full reproducibility. All tables and figures can generated using a single command-line script (run_all).

4. RESULTS AND DISCUSSION

4.1. Window A — Thiophene / n‑ octane / 30 ± 5 °C / 400–600 ppm

The subset Window-A is represented by six entries from three different studies (Table 1). In this stable operating window, the reported flux varies from 2.2 to 5.37 $kg \cdot m^{-2} \cdot h^{-1}$ and EF ranges from approximately 2.9 to 5.6. PDMS/MIL-101(Cr) (6 wt% loading) achieves the highest EF (≈ 5.6) with a high flux value of ≈ 5.2 $kg \cdot m^{-2} \cdot h^{-1}$). On the other side, neat PDMS/ceramic has a higher maximum flux (≈ 5.37 $kg \cdot m^{-2} \cdot h^{-1}$) with competitive EF (≈4.22). These two geometric configurations are located at a Pareto frontier corresponding to the simultaneous maxima of flux and EF (Table 4). Configuration level ordering for Window A also confirms these trends. According to the balanced performance list (min–max normalized mean flux×min–max normalized mean EF), PDMS/MIL-101(Cr) 6 wt% is ranked first followed by PDMS/Ni^{2+} Y 10 wt% and PDMS/Ni^{2+} Y 5 wt% (Tables 2–3). In general, within this operability window MOF-loaded PDMS membranes (MIL-101(Cr)) show the most promising flux–EF compromise. In the mean time, the PDMS membrane retains comparable pristine flux ceiling as the PDMS membrane supported on a ceramic substrate at similar feed condition and temperature. The mean values of flux and EF at the configuration level are shown in Fig. 4 and 5, respectively.

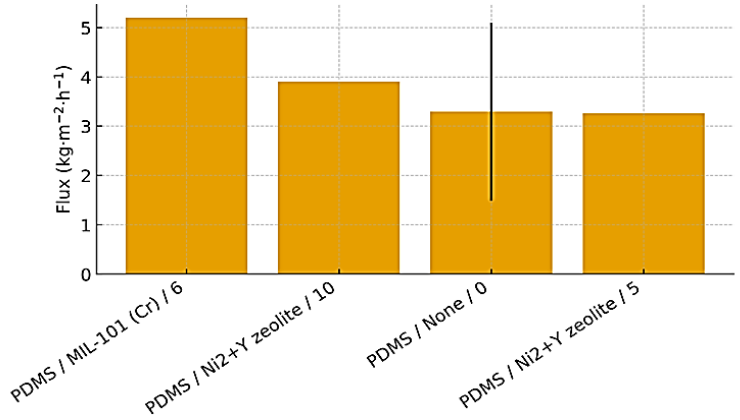

Fig. 4. Window A: Mean Flux ± SD by configuration.

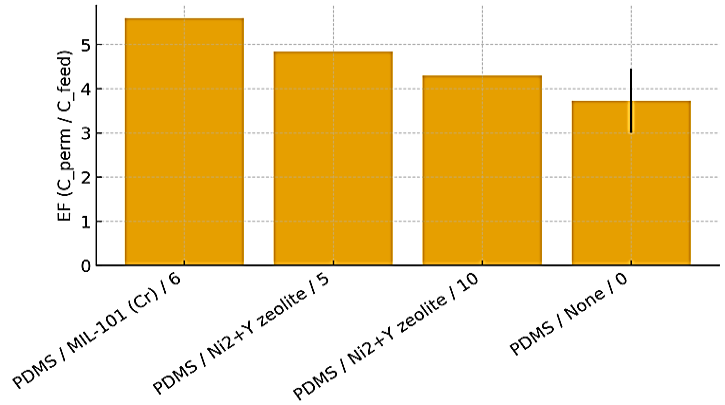

Fig. 5. Window A: Mean EF ± SD by configuration.

Table 1. Unified operating-window subset (Thiophene / n-octane / 30±5 °C, 400–600 ppm).

Polym.	Supp.	Fill.	wt%	Feed	Perm.	Pp	l	J	EF	Ref.
PDMS	PVDF	None	0	500	2030	3	14	2.2	4.06	Yu *et al.*, [22]
PDMS	PVDF	MIL-101(Cr)	6	500	2800	3	14	5.2	5.6	Yu *et al.*, [22]
PDMS	PS	None	0	500	1450	–	–	2.3	2.9	Li *et al.*, [21]
PDMS	PS	Ni^{2+} Y	5	500	2420	–	–	3.26	4.84	Li *et al.*, [21]
PDMS	PS	Ni^{2+} Y	10	500	2150	–	–	3.9	4.3	Li *et al.*, [21]
PDMS	Ceramic	None	0	400	1688	2.1	8	5.37	4.22	Li *et al.*, [21]

Note: All data correspond to Window A conditions (Thiophene/n-octane, 30 °C, 400–600 ppm). Pp = permeate pressure; l = selective-layer thickness; J = total permeate flux; EF = enrichment factor.

Table 2. Top-3 configurations ranked by a balanced score = norm(mean Flux) × norm(mean EF).

polymer	filler	Filler (wt%)	n	mean flux	max flux	mean EF	max EF	score balanced	Ref.
PDMS	MIL-101 (Cr)	6	1	5.2	5.2	5.6	5.6	1	Yu *et al.*, [22]
PDMS	Ni2+Y zeolite	10	1	3.9	3.9	4.3	4.3	0.10096489	Li *et al.*, [21]
PDMS	Ni2+Y zeolite	5	1	3.26	3.26	4.84	4.84	0	Li *et al.*, [21]

Table 3. Full leaderboard by configuration (polymer, filler, wt%).

polymer	filler	Filler (wt%)	n	Mean flux	Max flux	Mean EF	Max EF	Score balanced	Ref.
PDMS	MIL-101 (Cr)	6	1	5.2	5.2	5.6	5.6	1	Yu *et al.*, [22]
PDMS	Ni2+Y zeolite	10	1	3.9	3.9	4.3	4.3	0.10096489	Li *et al.*, [21]
PDMS	Ni2+Y zeolite	5	1	3.26	3.26	4.84	4.84	0	Li *et al.*, [21]
PDMS	None	0	3	3.29	5.37	3.72666667	4.22	0	Xu *et al.*, [23]

Table 4. Pareto-frontier points (maximize Flux & EF) within the unified window.

Polym.	Supp.	Fill.	wt%	Feed	Perm.	Pp	l	J	EF	Ref.
PDMS	PVDF	MIL-101(Cr)	6	500	2800	3	14	5.2	5.6	Yu *et al.*, [22]
PDMS	Ceramic	None	0	400	1688	2.1	8	5.37	4.22	Xu *et al.*, [23]

Note: Pareto points correspond to non-dominated configurations within Window A (Thiophene/n-octane, 30 ± 5 °C, 400–600 ppm). J = total permeate flux (kg $m^{-2} h^{-1}$); EF = enrichment factor; Pp = permeate pressure (mbar); l = selective-layer thickness (µm).

4.2. Window B — Thiophene / n‑heptane / 60 ± 5 °C / 400–600 ppm.

After making the selections (based on inclusion criteria/Window-A), Subset Window-B involves 4 records (single-study source; additional exclusions are zero). Subset (Table 4)

and leaderboard (Table 5) provide configuration-level performance summary; Pareto set (Table 6) is the non-dominated rows of all solutions in all activities–metabolites combinations matching this window in the design space. Although Window B operates at a higher temperature (60 ± 5 °C), observed flux values are overall low compared to those in window A due to differences in membrane material (all PEG based), fuel type, and an additional intrinsic transport resistance resulting from the higher operating temperature alone. For B configuration, summary results are given in Fig. 6 and 7. Because of the low sample size of B, these results are directional. Rankings are according to Table 5 and, in the fixed window case, no configuration outperforms with both Flux and EF any of the Pareto points listed (Table 6).

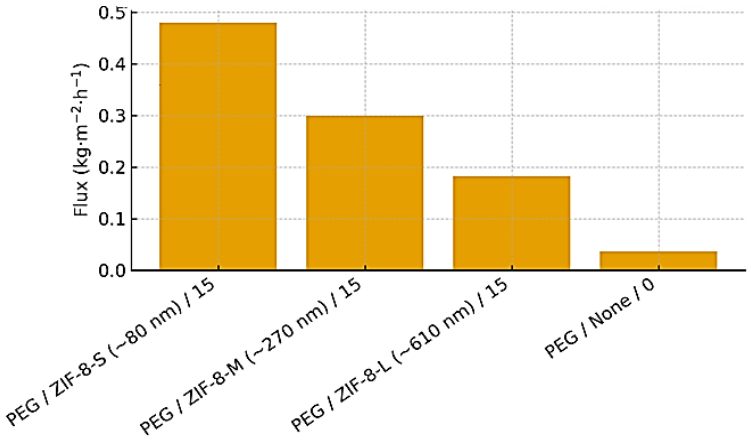

Fig.6. Window B: Mean Flux ± SD by configuration.

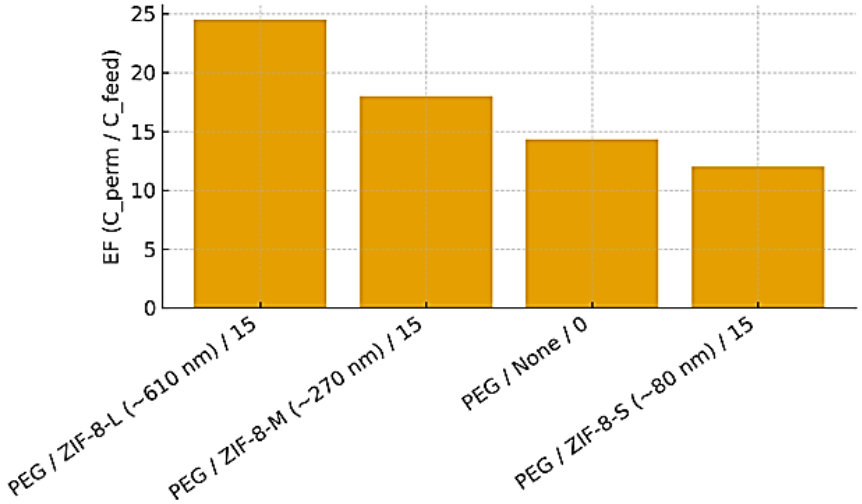

Fig.7. Window B: Mean EF ± SD by configuration.

After applying the fixed inclusion criteria, the Window-B subset comprised 4 rows (single-study source; no additional exclusions). Due to the small sample size, we will treat our estimates as directional. Compact Table 4 presents the key quantities in each row including citation, Flux, and EF. A higher level configuration ranking (Table 5, compact) is based on a balanced score represented by the product of mean Flux and EF in Window B min–max normalized per row subset; the complete and Pareto list are available in the Supplementary workbook for transparency. To mitigate over-interpretation from small n in Window B, we (i) report mean ± SD per configuration within each window, (ii) perform Pareto status at the row level and (iii) make publicly available a Supplementary workbook

featuring the full subset, leaderboard, Pareto list and machine-readable artifacts for reproducibility.

Table 4. Window B subset — essential fields only.

polymer	filler	wt%	Flux (kg·m^-2·h^-1)	EF	Ref
PEG	None	0	0.037	14.33	Zhan *et al.*, [24]
PEG	ZIF-8-L (~610 nm)	15	0.183	24.5	Zhan *et al.*, [24]
PEG	ZIF-8-M (~270 nm)	15	0.3	18.0	Zhan *et al.*, [24]
PEG	ZIF-8-S (~80 nm)	15	0.48	12.0	Zhan *et al.*, [24]

Table 5. Window B top configurations by balanced score— essential fields only.

configuration	polymer	filler	wt. %	n rows	N studies	mean Flux (kg·m^{-2}·h^{-1})	mean EF	score
PEG / ZIF-8-L (~610 nm) / 15	PEG	ZIF-8-L (~610 nm)	15	1	1	0.183	24.5	0.32957
PEG / ZIF-8-M (~270 nm) / 15	PEG	ZIF-8-M (~270 nm)	15	1	1	0.3	18.0	0.28497
PEG / None / 0	PEG	None	0	1	1	0.037	14.33	0.0

4.3. Cross-window comparison and practical relevance

An absolute value of the flux from one operating window cannot be directly compared to the other at A: pure n-octane, 30 °C or B: pure n-heptane, 60 °C because they are not conducted at the same feed and temperature. Whilst this restricts the range of joint design maps that can be formed, each window does exhibit uniform Flux–EF trade-offs. The relationship between the EF and fuel quality given by the one-stage mass balance (Eq. 6) is used to relate membrane properties with the relative sulfur removal that could be obtained in the retentate at realistic stage-cuts (θ). This offers a possibility of read-across between various membrane orientations. To screen and assess process relevance, a combined design plot (Flux vs. EF) with both windows included—using configuration specific markers scaled by filler wt%—is used to illustrate performance regions of interest. Superimposed removal-percentage isocurves at $\theta \in \{0.5\%, 1\%, 2\%, 5\%\}$) demonstrate the

transition on membrane performance towards a more retentive sulfur reduction (these comparisons are shown in Fig. 8 and 9).

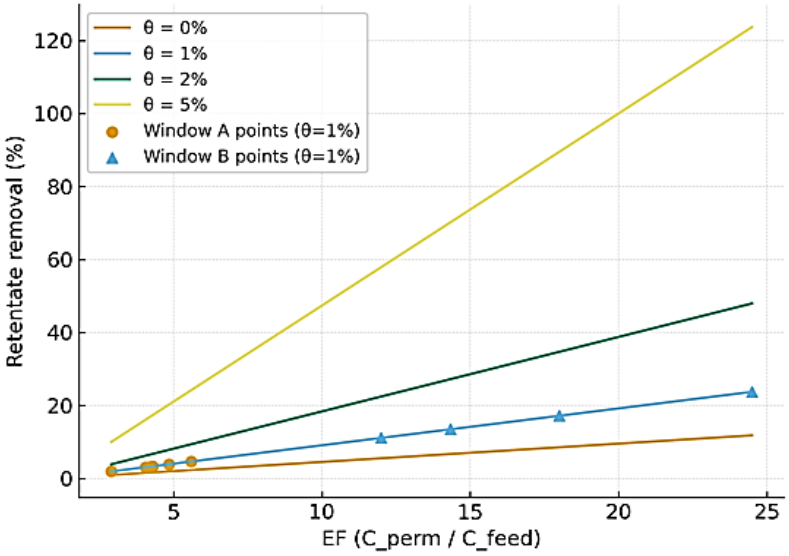

Fig.8. Flux–EF design map with Pareto frontiers in Windows A & B.

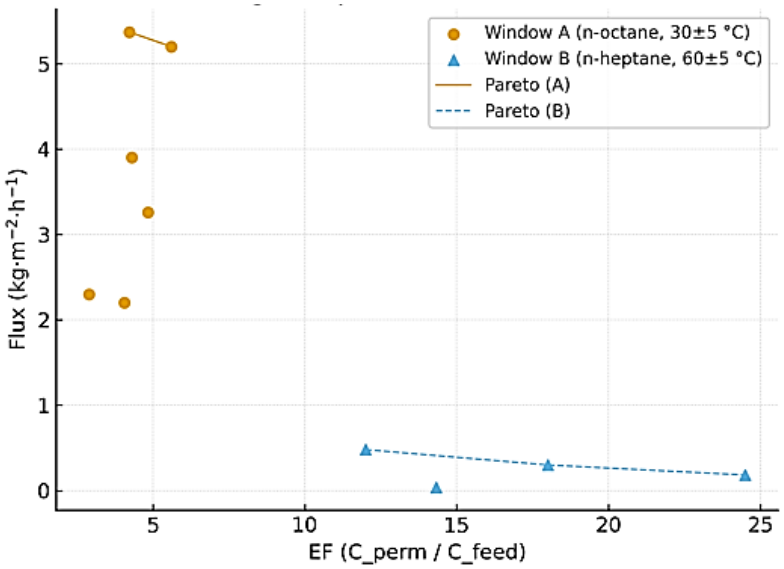

Fig.9. Practical removal map involve Removal % vs EF for θ.

This benchmarking strategy used by us represent a consistent approach to evaluating efficiency of pervaporation membranes for thiophenic sulfur removal. Through the use of normalized design maps combined with Pareto front analysis, the platform allows for a straightforward comparison of membrane performance within predefined operating windows, disclosing the inherent trade-off among permeation flux and enrichment factor. Although these trade-offs have been acknowledged in traditional membrane processes, the normalised benchmarking applied here reveals performance trends that can hardly be inferred from isolated experimental studies under different operating conditions. When compared against the literature-reported flux–selectivity trade-off envelopes and upper-bound trends for pervaporation desulfurization membranes, the optimal configurations

reported herein (e.g., MOF-based MMMs) are shown to approach but not surpass established performance limits. This validates that the gains are in line with established physical tradeoffs, and are not merely artifacts of selecting good data or tests.

The normalised data and the data in the operating windows investigated clearly present that MMMs have a superior performance compared to neat polymer membranes in terms of relative performances. It is important to note that this established superiority should not be considered as an ultimate or omnipresent advantage, rather than Pareto dominance within normalized (J–EF) membrane flux vs EF space with fixed operating windows, in terms of absolute or universally best performing membranes. The fact that MMM is often found in the Pareto front does not mean it will be invariably placed at a non-dominated region, as regions of this surface represent more promising trade-offs among the flux and enrichment factor for MMM, showing IFS (that arises from the interaction between inorganic fillers and selective sorption and permeation pathways). The fillers (e.g., MIL-101(Cr), Ni^{2+} -Y zeolite, and ZIF-8) can enhance the affinity for thiophenic sulfur compounds and maintain open transport pathways for C_1 –C_2 hydrocarbons; this finding is important, as improved flux and selectivity at the same time are seldom simultaneously achieved in single-polymer membranes.

However, the extent of performance enhancement in MMMs is extremely dependent on filler identity and its properties (particle size, dispersion quality, loading level). For example, the flux–selectivity compromise is particularly favorable for MIL-101(Cr)–based MMMs because of its high pore volume and strong sorption sites available towards thiophene, while zeolite-based MMMs generally exhibit higher selectivity gains but moderate increases in permeability. These findings underline that MMMs are not only determined by the chemistry of the fillers but, fabrication quality, polymer–filler interfacial compatibility also affect its performance.

Besides the membrane composition, characteristics of support play prominent role in defining achievable flux. Ceramic supports have lower mass transfer resistance than polymeric one (i.e., PVDF or PS) so, even in the absence of fillers neat PDMS membranes deposited on ceramic tend to be some of the highest flux capable within Window A. Nevertheless, the improved support permeability is not enough to completely neutralize the selective sorption that introduced by inorganic fillers, it can be seen from the fact that enrichment factors of supported neat polymer membranes are lower than those of MOF-loaded MMMs. This indicates that support tuning alone may not be sufficient to achieve optimal separation performance and also suggests flux boosting strategies depending solely on support design.

The systematic variation in the statistical features of different membrane sizes, shown here, is perhapsnot purely random but is due to variations in membranes fabrication,filler dispersion interfacing defects and thickness uniformity. When the dispersion of fillers is not ideal, or the polymer-filler interface is not perfect, inorganic fillers could be less effective as a function of model parameters than expected based on primary principles. These observations show the importance for using uniform fabrication techniques and comprehensive description of membrane preparation conditions. Being one of the drivers behind the development of an industry standard benchmarking framework as proposed in this work.

From an industry vison, the interpretation of enrichment factor into practical sulfur removal with stage-cut thoughts is a more meaningful description of membrane performance. While high enrichment factors are desirable, industrial operation is based on the compromise between selectivity and flux at making economic sense membrane areas. In this sense, the membranes as moderate selective ones but with high flux can be also able to arrive practically same removal of sulfur by working in their cut-off conditions as well as they still are meaningful indicators for deep desulphurisation or polishing stages with ultra-low sulphur requirement or using membrane modules on hybrid separation schemes, due to its higher enhancement factors and relatively a lower degree of enrichment. This self-evident discovery implies that membrane design will focus on the balance of performance rather than maximizing one single metric.

The results of this study, however, are inherently limited by the scarcity and non-uniformity of available literature data within the planned operating windows with respect to detailed mass, volume fractions, sizes etc. in particular for Window B; therefore such trends should be considered relative and indicative rather than absolute or applicable to an entire population. The oper ating windows considered are pre-defined, and hence the trends cannot be directly extrapolated to all possible fuels and operation conditions; however, as these represent some of the most frequently reported operating conditions in the literature, their comparative trends make sense for benchmarking purposes. Thus, the proposed framework is flexible and easily expandable with any new operating windows when more diverse, systemically-reported data are available.

All considered, this research shows that MMMs with MOF fillers have high potential for upscaling in pervaporative fuel desulfurization under a consistent and comparative basis approach. Nevertheless, they are highly sensitive to morphology control and disperson quality. The benchmarking and Pareto-based approach we have described here represent powerful tools with which to identify meaningful performance gains, as well as to inform the rational design of next-generation membranes by the industry.

5. CONCLUSIONS

This work suggested a consistent, data-driven benchmarking outline for assessing pervaporation membranes in the situation of sulfur removal from fuels. This method includess design mapping, Pareto dominance relationshipss in the (J,EF) performance space and transparent rank ordering to allow for fair cross-comparison of membrane systems considered within a common operating window.

From a technical perspective, the findings suggest that MOF-based mixed matrix membranes (MMMs) possess the most desirability balance between permeation flux and enrichment factor in terms of the given operating windows. Relatively, these systems are superior to neat polymer membrane and non-MOF-filled MMMs, revealing that they can be pushed off further on the Pareto frontier. The method allows the non-dominated operating points to be instantly discovered, performance trade-offs between membrane supports and active materials to be demystified, and a uniform platform for analytical comparison of otherwise disparate literature to be established. Through the simultaneous development of contourlines for enrichment factor vs. retentate S removal in a single mass balance, qualitative selectivity metrics are converted into process relevant and functionally meaningful targets for early-stage process synthesis and membrane screening.

All data, figures and scores presented in this study are available as part of the machine-accessible datasets (available in public domain) deposited with a publicly available repository. This will allow to have an open, traceable and reproducible benchmark results. While the framework inherently involves accepting base-case assumptions about membrane support properties and is limited by an uneven coverage of literature data, it is robust and reveals significant knowledge deficits which affect material choice.

In the future, we will further develop this framework by incorporating activity-based sorption models to better represent thermodynamic–transport interactions; using mixed-effects statistical methods to address variation in membrane type and source study factors; and validating our benchmarking approach with prospectively generated data that have been acquired over well-defined operating windows. Even if certain membranes exhibit relatively low flux, but with very high selectivity towards some of these sulfur species, they might still be technically important. These are particularly well suited for tailcleaning applications or blending with hybrid desulfurization processes where selectivity might be favored over throughput. In sum, the proposed ranking framework presents a systematic system for membrane screening and optimization that enables data-driven material design and eases more efficient industrial deployment of pervaporation-based sulfur removal technologies.

DATA AND CODE AVAILABILITY

All tables and figures in this paper are both inline-reported as well as in the working directory (e.g., paper_rows_cleaned_with_EF. csv). csv, window sub-sets, leaderboards and Pareto CSVs and Supplementary_Data_Subset. xlsx) are not publicly available, but may be made available upon reasonable request to the corresponding author.

ACKNOWLEDGMENTS

The authors appreciate the support of the University of Babylon and a conducive research environment throughout this study.

REFERENCES

[1] Mamuad, R.Y. and Choi, A.E.S. " Biodesulfurization Processes for the Removal of Sulfur from Diesel Oil: A Perspective Report, " *Energies*, Vol.16,No.6, p. 2738, 2023. https://doi.org/10.3390/en16062738.

[2] Esmaeili-Faraj, S. H., Jafari, M., and Kazemimoghadam, M. " Diesel fuel desulfurization by alumina/polymer nanocomposite membrane: Experimental analysis and modeling by the response surface methodology, " *Chemical Engineering and Processing - Process Intensification*, Vol.164, 2021. https://doi.org/10.1016/j.cep.2021.108396.

[3] Mortaheb, H.R., Ghaemmaghami, F. and Mokhtarani, B. " A review on removal of sulfur components from gasoline by pervaporation, " *Chemical Engineering Research and Design*, Vol.90,No.3, pp. 409–432, 2012. https://doi.org/10.1016/j.cherd.2011.07.019.

[4] Roostaiy Ghalehnooiy, M., Marjani, A. and Ghadiri, M. " Synthesis and characterization of polyurethane/poly(vinylpyridine) composite membranes for desulfurization of gasoline, " *RSC Advances*, Vol.5,No.116, pp. 95994–96001, 2015. https://doi.org/10.1039/C5RA13951A.

[5] M. Salman, M. Rezakazemi, T. Mohammadi, and M. Shakouri, " Advances in the Applications of Mixed Matrix Membranes for Desulfurization of Transportation Fuels, " *Separation & Purification Reviews*, Vol.53,No.4, pp. 448–474, 2024. https://doi.org/10.1080/15422119.2024.2322425.

[6] Hong, S., Lan, Y., Zhang, Y., Fu, B., and Peng, P." Enhanced Pervaporative Desulfurization Performance of PDMS Membranes by Biomineralization, "*Journal of Applied Polymer Science*, Vol.143, No.5, 2026. https://doi.org/10.1002/app.58161.

[7] X. Han, J. Liu, Q. Zhao, X. Lu, and J. Deng," Improved desulfurization performance of polydimethylsiloxane membrane by incorporating metal organic framework CPO-27-Ni, " *Separation and Purification Technology*, Vol. 217, pp. 86–94, 2019. https://doi.org/10.1016/j.seppur.2019.01.075.

[8] C. Cai, J. Liu, X. Han, S. Ren, and Y. Zhang, " Improved desulfurization performance of polyethyleneglycol membrane by incorporating metal organic framework CuBTC, " *Polymers*, Vol.12,No.2, 2020. https://doi.org/10.3390/polym12020414.

[9] Abdali, A., Mahmoudian, M. and Nozad, E. " Desulfurization of a Model Fuel using Pervaporation Membranes Containing Zn-MOFs, " *Journal of Polymer Research*, Vol.28,No.7, 2021. Available at: https://doi.org/10.1007/s10965-021-02472-7.

[10] Z. Wang, G. Sun, S. Yang, Z. Wang, J. Yang, and K. Wang, " Preparation and Properties of Polyimide/Polysulfonamide/Polyethylene Glycol (PI/PSA/PEG) Hydrophobic Nanofibrous Membranes, " *Materials*, Vol.17, No.16, pp. 4135, 2024. Available at: https://doi.org/10.3390/ma17164135.

[11] R. Qi, J. Chen, J. Li, and J. Sun, " Pervaporative desulfurization of model gasoline with Ag2O-filled PDMS membranes, " *Separation and Purification Technology*, Vol.57,No. 1, pp. 170–175, 2007 . https://doi.org/10.1016/j.seppur.2007.04.001.

[12] S. Shahid, K. Nijmeijer, I. Németh, and M. Wessling," MOF-mixed matrix membranes: Precise dispersion of MOF particles with better compatibility via a particle fusion approach for enhanced gas separation properties, " *Journal of Membrane Science*, Vol.492, pp. 21–31, 2015. https://doi.org/10.1016/j.memsci.2015.05.015.

[13] F. Wu, S. Yan, J. Yu, C. Wang, and G. Zhang," High-performance UiO-66-NH2 tubular membranes by zirconia-induced synthesis for desulfurization of model gasoline via pervaporation, " *Journal of Membrane Science*, Vol. 556, pp. 54–65, 2018. https://doi.org/10.1016/j.memsci.2018.03.090.

[14] S. Li, X. Jiang, S. Wang, X. Zhao, and L. Wang, " Recent Advances in Polymer-Inorganic Mixed Matrix Membranes for CO2 Separation, " *Polymers*, Vol.13,No.15, p. 2539, 2021. https://doi.org/10.3390/polym13152539.

[15] Kadhum, A.T. and Albayati, T.M. " Desulfurization techniques process and future challenges for commercial of crude oil products: Review, " Vol.2443,No.1, p. 030039, 2022. https://doi.org/10.1063/5.0092049.

[16] H. B. Park, J. Kamcev, L. M. Robeson, B. D. Elimelech, and B. D. Freeman, "

Maximizing the right stuff: The trade-off between membrane permeability and selectivity, " *Science*, Vol.356,No.6343, 2017. https://doi.org/10.1126/science.aab0530.

[17] A. Gasós, N. S. Patel, B. S. Sholl, and R. P. Lively," Process performance maps for membrane-based CO2 separation using artificial neural networks, " *International Journal of Greenhouse Gas Control*, Vol.122, p. 103812, 2023. https://doi.org/10.1016/j.ijggc.2022.103812.

[18] N. Hara, T. Yamaguchi, and M. Nomura," Bi-Objective Optimization of Techno-Economic and Environmental Performance for Membrane-Based CO2 Capture via Single-Stage Membrane Separation, " *Membranes*, Vol.15,No.2, p. 57, 2025. https://doi.org/10.3390/membranes15020057.

[19] Lin, L., Zhang, Y. and Kong, Y. " Recent advances in sulfur removal from gasoline by pervaporation, " *Fuel*, Vol.88, No.10, pp. 1799–1809, 2009. https://doi.org/10.1016/j.fuel.2009.03.031.

[20] Cao, X., Wang, K. and Feng, X. " Mass transfer fundamentals in pervaporation, perstraction and sorption: A unified approach, " *Chemical Engineering Research and Design*, Vol.204, pp. 282–291, 2024. https://doi.org/10.1016/J.CHERD.2024.02.045.

[21] B. Li, G. Zhang, S. Zhang, Q. Liu, and Y. Lin," Pervaporation performance of PDMS-Ni2+Y zeolite hybrid membranes in the desulfurization of gasoline, " *Journal of Membrane Science*, Vol.322,No.2, pp. 293–301, 2008. https://doi.org/10.1016/j.memsci.2008.06.015.

[22] S. Yu, B. Fu, J. Wang, L. Zhao, C. Liu, J. Zhang, H. Wu, and Z. Jiang," Enhanced pervaporation performance of MIL-101 (Cr) filled polysiloxane hybrid membranes in desulfurization of model gasoline, " *Chemical Engineering Science*, Vol.135, pp. 479–488, 2015. https://doi.org/10.1016/j.ces.2014.11.058.

[23] R. Xu, S. Zhang, Y. Lin, G. Zhang, and Q. Liu, " Pervaporation separation of n-octane/thiophene mixtures using polydimethylsiloxane/ceramic composite membranes, " *Desalination*, Vol.258,No.(1–3), pp. 106–111, 2010. https://doi.org/10.1016/j.desal.2010.03.035.

[24] X. Zhan, Z. Wang, G. Sun, X. Zhan, Y. Lin, and J. Yang, " Enhanced Desulfurization Performance of ZIF−8/PEG MMMs: Effect of ZIF−8 Particle Size, " *Membranes*, Vol.13,No.5, p. 515, 2023. https://doi.org/10.3390/MEMBRANES13050515/S1.